Int. J. Electrochem. Sci., 12 **(2017)** 4056 – 4076, doi: 10.20964/2017.05.47

International Journal of
ELECTROCHEMICAL
SCIENCE
www.electrochemsci.org

Effect of Calixarene Sulfonic Acids Hydration on Their Proton Transport Properties

Lyubov Shmygleva[1,*], *Nikita Slesarenko*[1], *Aleksander Chernyak*[1,2], *Evgeny Sanginov*[1], *Aleksander Karelin*[1], *Anna Pisareva*[1], *Rostislav Pisarev*[1], *Yury Dobrovolsky*[1]

[1] Institute of Problems of Chemical Physics of RAS, 1 Academician Semenov Avenue, Chernogolovka, Moscow region, Chernogolovka, Russia, 142432
[2] Science Center in Chernogolovka RAS, 9 Lesnaya str., Chernogolovka Moscow Region, 142432
[*]E-mail: shmygleval@mail.ru

Received: 18 November 2016 / *Accepted:* 19 January 2017 / *Published:* 12 April 2017

The influence of the morphology of calix(n)arene sulfonic acid hydrates with different number of aromatic rings (n = 4, 6, 8) on their proton transport properties was studied. Simultaneous thermal analysis, IR spectroscopy, X-ray powder diffraction and nuclear magnetic resonance were used for investigating of proton hydrate shell, water content and structure features. It was shown that studied calix(n)arene sulfonic acids hydrates have high proton conductivity up to 10^{-1} S/cm.

Keywords: Calixarene sulfonic acids, water content, proton conductivity, activation energy, NMR study.

1. INTRODUCTION

Solid electrolytes with effective proton transport at low temperatures are of a great interest from both fundamental and practical viewpoints.

The majority of proton conductors based on organic compounds are crystalline hydrates, in which water molecules are involved in proton transport due to the formation and destruction of bound proton forms. Despite the considerable amount of theoretical and experimental data on the crystal and proton hydration shell structure and peculiarities of proton transport in various materials, there is no consensus of opinion on the nature and mechanisms of proton transport in such systems.

On the other hand, the creation of new solid state electrochemical devices (fuel cells, supercapacitors, batteries, and sensors for determining the composition of gases and liquids) requires the development of new materials, in which high proton conductivity should be retained over a wide range of ambient temperatures and humidity and imposed potentials [1, 2].

There is a large class of compounds called calixarenes, which have a layered structure with rigid fragments of the organic framework alternating with the layers formed by the proton-generating groups surrounded by a significant amount of crystallization water [3]. Earlier, we showed [4–7] that effective ionic transport appears in these compounds, leading to the production of substances with record proton conductivity.

Chemistry of calixarene with 4 aromatic rings is the most developed. These compounds are the most stable in the viewpoint of conformational transition. But there is no any data about the calix(4)arene sulfonic acid in literature. All known its sulfonates are hydrates, which can contain up to 16 water molecules per molecule of calixarene [8–15]. But unlike calix(4)arenes the chemistry of another calix(n)arenes, such as for n = 6 and 8, is less developed. Although the structure of calix(6)arene sulfonic acid was established [16].

Therefore, here we studied the influence of the morphology of calix(n)arene sulfonic acids with different number of aromatic rings (n = 4, 6, 8) on their proton transport properties.

2. MATERIALS AND METHODS

2.1 Materials

Calix(n)arene sulfonic acids (**SCn**, n = 4, 6, 8) were synthesized by sulfonation [17] of the starting calix(n)arenes, which was purchased from Sigma Aldrich and Acros. All the samples were dried over P_2O_5 and then kept in exsiccator with different relative humidities (**RH**) for at least one week.

2.2 Thermal stability

Thermal stability of the samples was determined by (**STA**) with mass spectrometric analysis of the decomposition products on Netzsch STA 409 PC Luxx® and QMS 403 C Aëolos instruments. The thermogravimetric analysis (**TGA**) and differential scanning calorimetry (**DSC**) curves were recorded in the temperature range 25–250 °C under argon atmosphere at the heating rate 5 °C/min.

2.3 IR spectroscopy

The prepared samples were analyzed using IR absorption spectroscopy (vacuum FTIR spectrometer Vertex 70V), IR ATR spectroscopy (diamond crystal from Bruker company) and Raman spectroscopy (Vertex 70V with RAMII module, λ = 1064 nm) with resolution 4 cm^{-1}.

*2.4 X-ray Powder Diffraction (**XRD**)*

XRD patterns were registered on an X-ray diffraction meter ADP-2-01 (Cu K_α-radiation, Ni filter) using X-RAY software for automation of obtaining, processing and analysing the data obtained

from x-ray diffraction from a DRON series. The approach increment of the detector block was 0.050, and the exposure time as 2 sec.

2.5 Impedance spectroscopy

The proton transfer parameters of the powder samples were determined by impedance spectroscopy in a temperature range of +70 – -50 °C at 10 – 75% RH. Equilibrium with the environment was monitored over the course of several days based on stabilization of the cell resistance. The frequency dependence of the sample impedance was obtained on Z-3000 impedance meter (Elins LLC, Russia) in a frequency range 1 Hz – 3 MHz with measurement signal amplitude of 10–100 mV. The proton conductivity of the samples was calculated by approximating the spectra of the experimental cell according to the equivalent circuit described in detail in [4].

*2.6 Nuclear magnetic resonance (**NMR**)*

The ^{13}C mass angel spinning (**MAS**) NMR spectra were measured with a Bruker AVANCE III 400MHz spectrometer at Larmor frequency of 100.6 MHz at room temperature. A Bruker MAS probe head with a 3.2 mm zirconia rotor was used. The frequency scale of the spectrum was expressed with respect to neat tetramethylsilane by adjusting the signal of solid adamantane spinning at 8 kHz to 38.48 ppm (^{13}C (^{1}H - decoupling) spectrum). Conventional cross-polarization (**CP**) experiments were used for the acquisition of the ^{13}C spectra with spinning rate 13 kHz. Experimental NMR parameters used for the acquisition of the ^{13}C CPMAS experiments: ^{1}H $\pi/2$ pulse, 2.5 μs, contact time was between 500 to 2000 μs, ^{1}H RF field for decoupling - 100 kHz with SPINAL-64, linear ramp 70–100%, acquisition time 36 ms, duration time 6s, number of scan 12000.

The self-diffusion coefficients were measured on ^{1}H nuclei by pulsed field gradient technique at the frequency of 400 MHz. The measurements were carried out on Bruker Avance-III – 400MHz NMR spectrometer, equipped with the diff60 gradient unit (the maximum field gradient amplitude was 60 T/m) at room temperature. The stimulated spin-echo technique was applied. The details of self-diffusion coefficients measurements are given in [18]. Experimental NMR parameters of pulse sequences: ^{1}H $\pi/2$ pulse 7.75 μs, gradient strength was varied linearly in 64 steps with maximum field gradient amplitude g – 40 T/m, duration gradient pulse δ 1–1.5 ms, the diffusion time t_d varied from 20 to 100 ms, repetition time 3c.

3. RESULTS AND DISCUSSION

3.1 Water content

Water content of studied samples was obtained from TGA and gravimetry. These two methods gave the similar results. Dependencies of water molecule number pur sulfonic group m on relative humidity for each SCn are shown on Fig. 1. From the extrapolation of the dependences we can assume

that in dry atmosphere studied samples are hydretae with m = 1. This assumption was confirmed by DSC and IR spectroscopy. At the low humidity of 10% RH for all studied compounds m = 2, process of hydration consists of three stages and is described by a linear equation (1). Coefficients a and b are listed in the table 1.

$$m = a + b \cdot RH \quad (1)$$

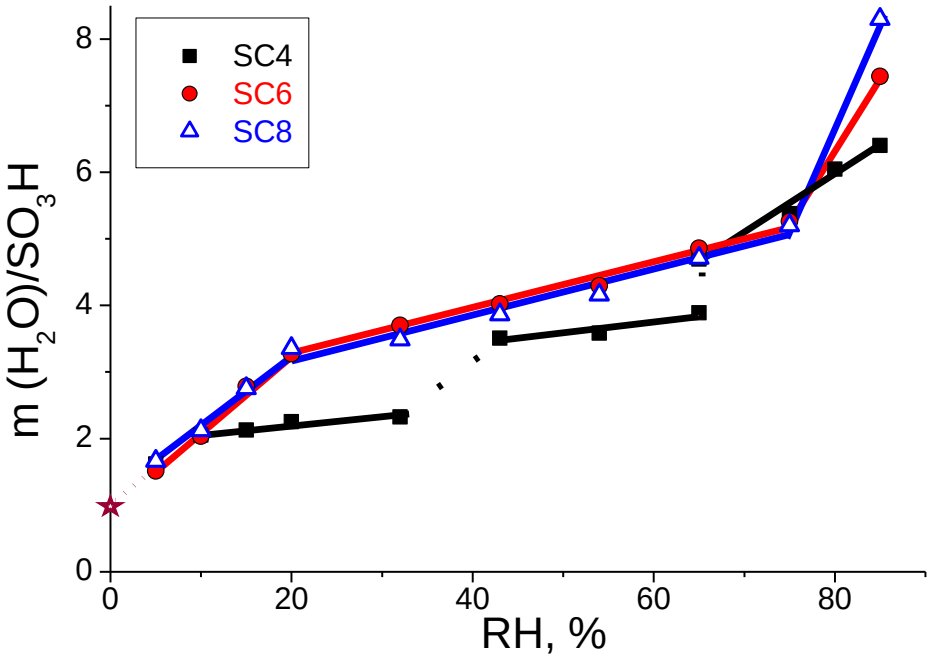

Figure 1. Dependencies of water molecule number per sulfonic group of SCn on RH (room temperature).

In our previous work [7] it was shown that at low humidity SC4 is tetrahydrate, but further data of NMR research and a more thorough TGA analysis indicate on two times more number of water. Two stable hydrates were observed for SC4: 2.0 – 2.3 H_2O molecules per SO_3^- group at humidity of 10 – 32 rel. % and ~ 3.5 at 43 – 65 rel. %. Further wetting led to a linear increase in the number of water molecules to 6.4 at 85 rel. %.

Table 1. Coefficients a and b of the equation (1) for three-stage hydration process of SCn.

	I			**II**			**III**		
	RH, %	***a***	***b***	**RH, %**	***a***	***b***	**RH, %**	***a***	***b***
SC4	15–32	1.95	0.012	43–65	2.72	0.017	> 65	-1.04	0.088
SC6	5–20	0.89	0.121	20–75	2.53	0.035	> 75	-11.10	0.218
SC8	5–20	1.05	0.114	20–75	2.49	0.034	> 75	-18.02	0.310

In our previous work [7] it was shown that at low humidity SC4 is tetrahydrate, but further data of NMR research and a more thorough TGA analysis indicate on two times more number of water. Two stable hydrates were observed for SC4: 2.0 – 2.3 H_2O molecules per SO_3^- group at humidity of 10

– 32 rel. % and ~ 3.5 at 43 – 65 rel. %. Further wetting led to a linear increase in the number of water molecules to 6.4 at 85 rel. %.

Unlike SC4, hydration processes of the samples with 6 and 8 aromatic rings during their wetting have another, but similar to each other, character: 3 stages of growth of water molecules are observed. Short intensive initial stage up to 20 rel. % leads to a rapid linear increase of *m* to 3.3 (*b* = 0.11–0.12). Further wetting followed by replacing this stage by a long part, while increase of the water number slows with increasing of RH (*b* = 0.034–0.035) and reaches ~ 5 molecules H_2O per sulfonic acid group from 20% to 75% RH. Humidification to 85% RH leads to a sharp increase in water followed by dissolution of SCn in their own crystal water. It should be noted that the number of molecules for such dissolution is directly proportional to the number of benzene rings *n* in SCn molecule. The amount of water was confirmed by STA data. Overall, the results are in a good agreement to the previously obtained in work [19].

3.2 Thermal stability

Figure 2 shows the DSC data of SCn kept at different humidity levels. In the region of degidration, DSC curves of SCn contain 1, 2 or 3 peaks. The number of peaks dependents on RH and amount of aromatic rings *n*. The transition to a two-step process of dehydration occurs at 5%, 10% and 15% RH for respectively SC4, SC6 and SC8. The stepwise loss of water from the SCn indicated that some portion of the water is loosely bound while the rest is involved in strong interactions with the SCn molecules in the crystal lattice.

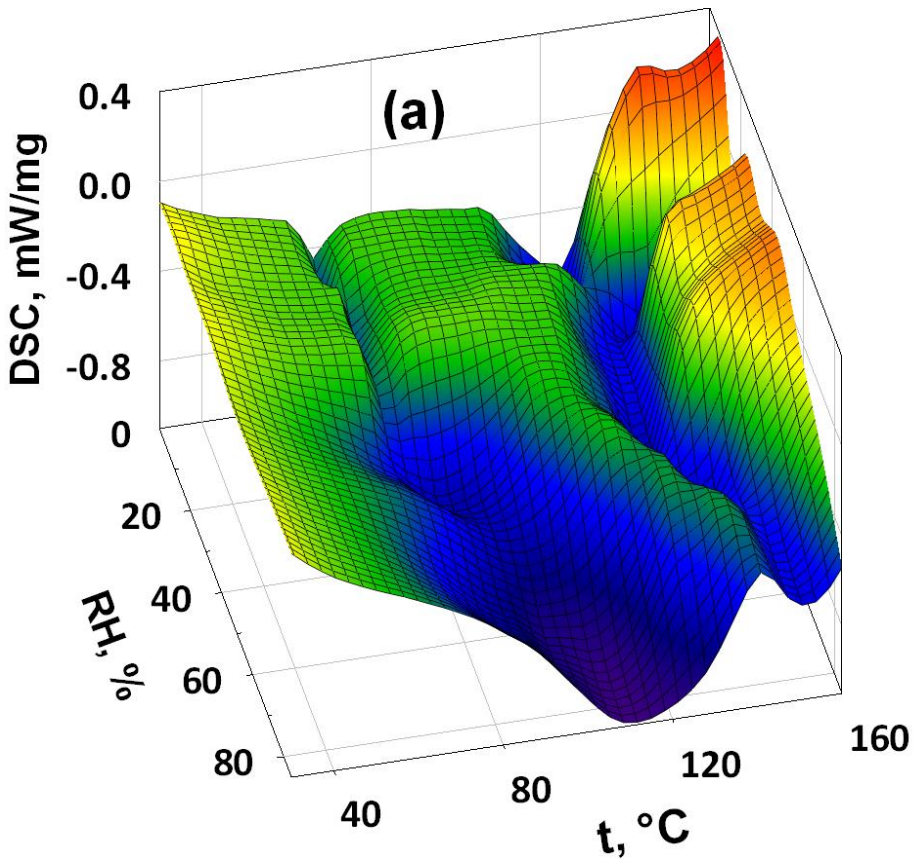

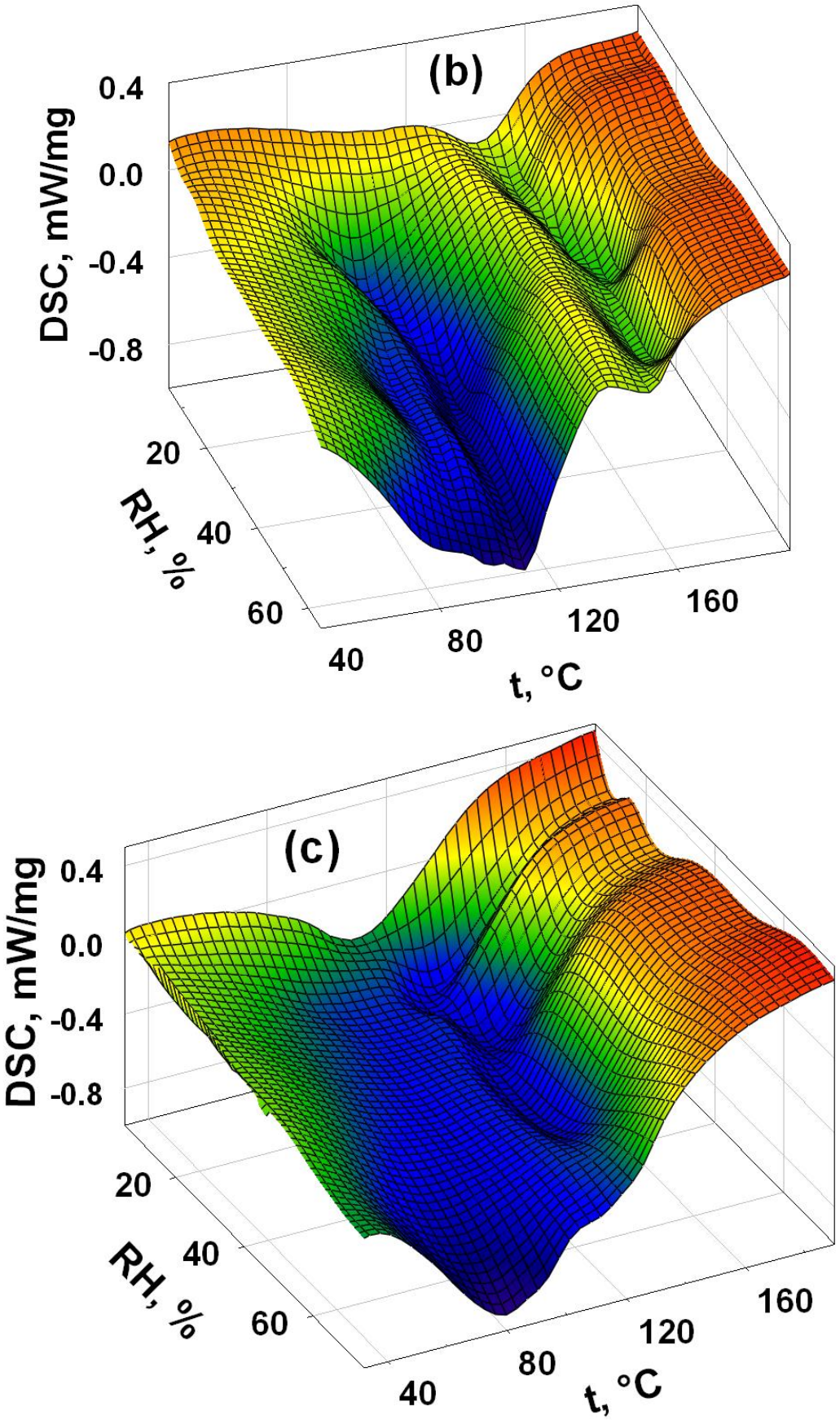

Figure 2. Variation of the DSC curves of SCn hydrates: SC4 (a); SC6 (b); SC8 (c).

For SC4 and SC8 only two peak of the water loss occur throughout the humidity range. The first peak with a maximum at t < 100 °C increases in the width and intensity with RH increasing, and corresponds to the removal of weakly bounded water molecules. A similar phenomenon is observed for SC6 compound, but instead of a single peak with a maximum at ~ 100 °C the third one appears at lower temperatures beginning with 32% RH.

The last DSC peak of strongly bounded water loss is located in the region of 120 – 150 °C. The intensity of it is corresponding to 1 H_2O per sulfonic group and do not change with RH increasing. Therefore, our previous assumption was correct. SCn hydrates with *m* = 1 are the most stable compounds and dehydration occurs in several stages: at first, higher hydrates transform respectively into tetra-, hexa- or octahydrate, and then the sample is completely dehydrated.

Melting of SCn with decomposition of anions occurs upon heating above 250 °C [19]. Decomposition of sulfonic groups of the acids above 250 °C is confirmed by the discovery of decomposition products of sulfonic group in the mass spectra.

3.3 IR spectroscopy

The results of IR spectroscopic study of SCn as function of the relative humidity are presented in Fig. 3. The aim of this research was to study the structural features of proton hydration shell at different levels of humidity. Spectra for all the samples have the same type on the condition of samples storing at the same humidity.

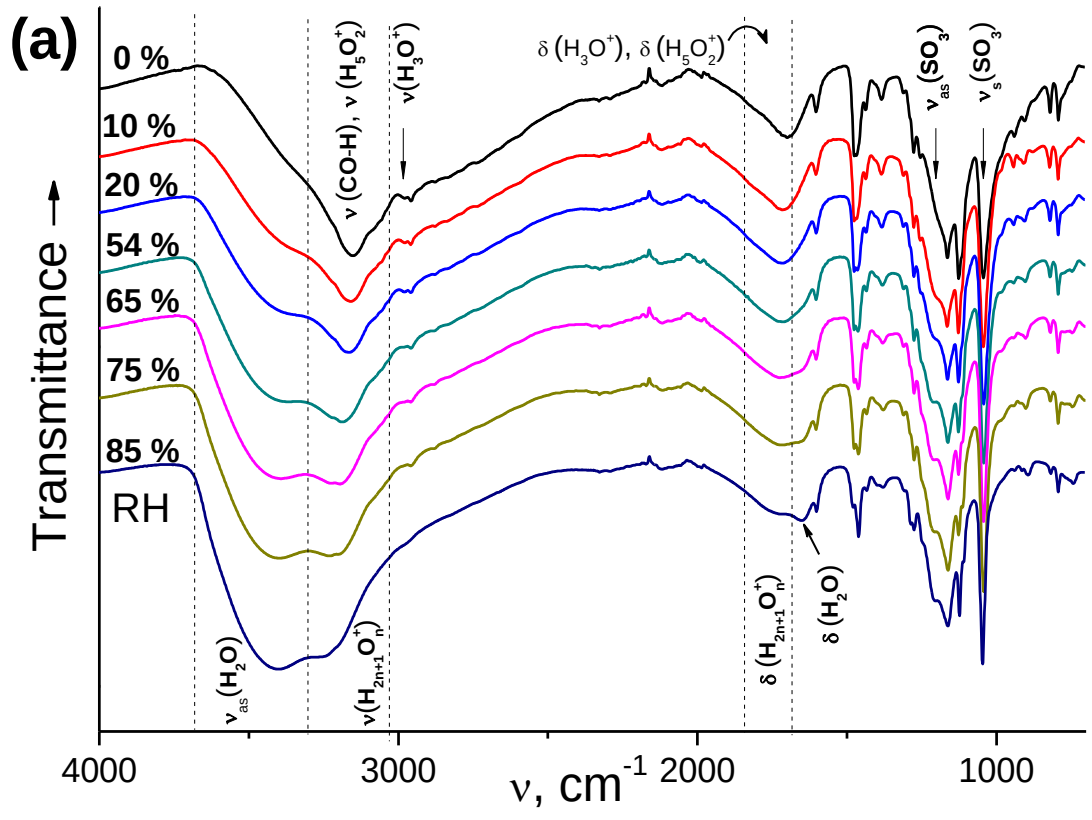

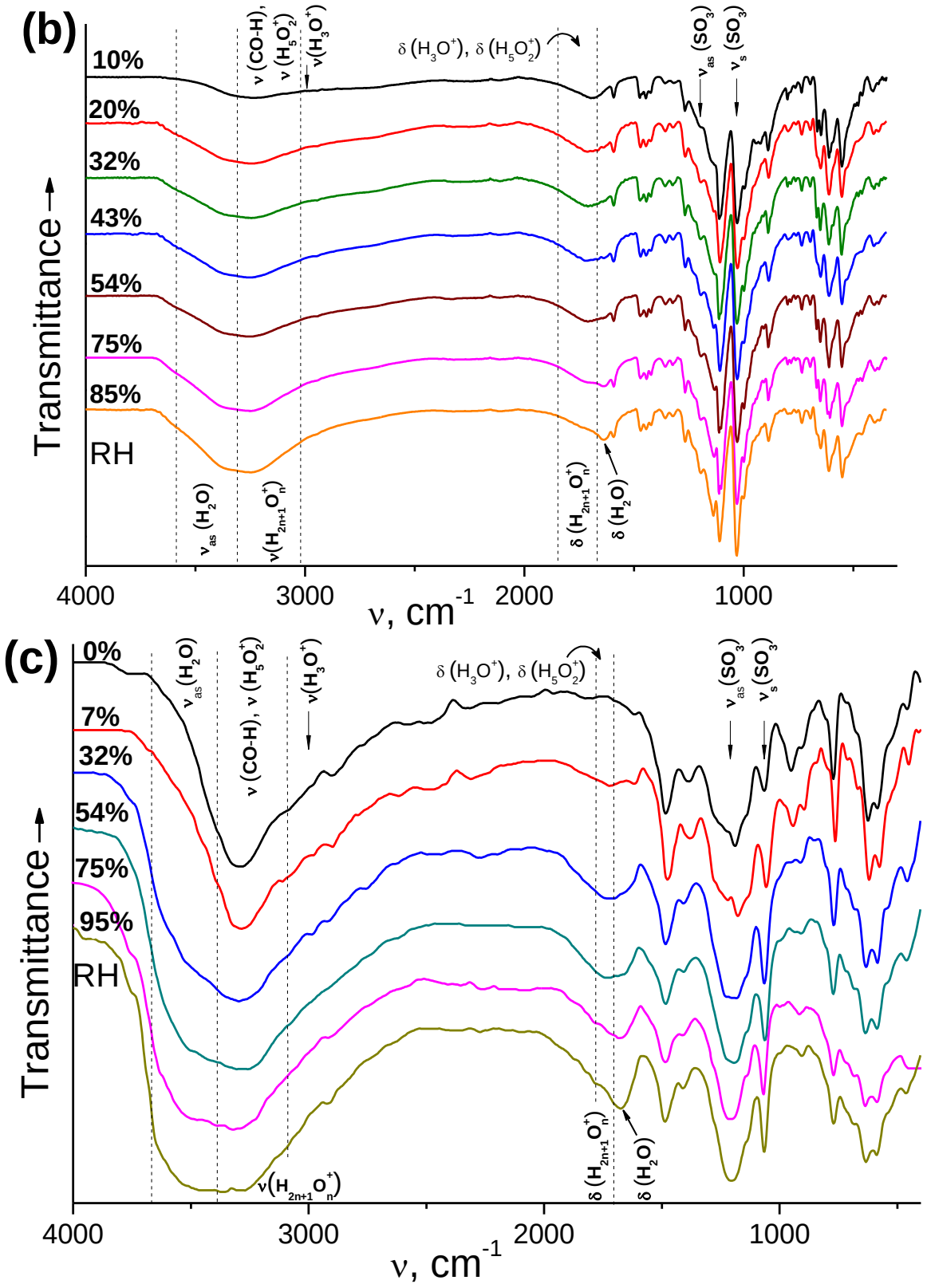

Figure 3. IR absorption spectra of SCn hydrates at different humidities: SC4 (a); SC6 (b) and SC8 (c).

The observed spectral differences are caused by subtle details of a three-dimensional framework structure. Individual features are manifested in the form of small frequency shifts, and disturbances in intensity of bands below 1600 cm^{-1}. This region is corresponded to the vibrations of the

aromatic rings and the bridging fragments. The area also includes bands of sulfonic group stretching and deformation vibrations, responsible for the state of the ionized or not state of acid. Bands of the ionized sulfonic groups are observed at all investigated RH values for all the samples. The following frequency values correspond to the symmetric and anti-symmetric stretching vibrations of S=O bonds of the $C–SO_3^-$ group (cm^{-1}):

	$\nu_s(SO_3)$	$\nu_{as}(SO_3)$
SC4	1044	1202 ± 3
SC6	1033	≤ 1198 (?)
SC8	1050	1210 ± 10

Similar intensive bands were observed in this field of IR spectra for the various polycrystalline and non-crystalline benzene sulfonic acids [20-24]. FTIR spectra of non-sulfonated calix[n]arenes (*n* = 4 and 6) in KBr pellets were published in works [25, 26]. So, we can compare spectroscopic data for the initial substance and its sulfonation product. A comparison shows that the sulfonation leads to relative small perturbation (within 30 cm^{-1}) of many vibtrational levels of the SC4 and SC6 molecules.

The contours of the bands $\nu_s(SO_3)$ and $\nu_{as}(SO_3)$ are modified due to the superposition of the phenolic group bands ν(C–C) and ν(C–O). There is a possibility of mixing of S–O, S–C and C–C vibrations. The strong $\nu_{as}(SO_3)$ band is observed approximately at 1200 cm^{-1} in the SC4 and SC8 spectra. However it did not occur in the SC6 spectrum on the background absorption of aromatics. So, its frequency is determined very approximately.

Decreasing of RH to 10% accompanied by the appearance of the weak bands at about 900–936 cm^{-1} related to the stretching vibration of S–O unionized sulfonic group $C–SO_2–OH$ in the SC6 and SC8 spectra (Fig. 3b, c). Protolytic equilibrium between unionized and ionized sulfonic groups is shifted towards the formation of the latter. Moreover, in SC4 group $C\text{-}SO_2\text{-}OH$ is not detected at all at RH = 10% and even at RH = 0% under vacuum (Fig. 3a). The dehydration of SC4 stops at the tetrahydrate formation (*m* = 1) as evidenced on the appearance of H_3O^+ broad bands ν(OH) at 3000 cm^{-1} and δ(HOH) mid broad band at 1690 cm^{-1}. The same bands of H_3O^+ ions are observed also in the SC6 and SC8 spectra at RH < 10%. At RH ≥ 10% the H_3O^+ bands disappear and the $H_5O_2^+$ bands appear. A broad band ν(OH) of $H_5O_2^+$ is screened by the ν(OH) band of the C–OH group whereas a mid broad δ(HOH) band shifts to 1715 cm^{-1}. At the higher RH there are favorable conditions for the higher proton hydrates formation. However, their definition is very difficult due to small spectral differences between them and the $H_5O_2^+$ ions. The estimated hydration $H_5O_2^+$ ions in the high humidity conditions followed by a slight shift of the maximum of δ(HOH) band to high frequencies.

The deformation C–C and C–O bands are expected below 700 cm^{-1}. The bending SO bands are observed also in this area. The spectra in this range were obtained only for SC6 and SC8 samples (Fig. 3b, c). One of the two moderate intensity bands with maxima at 553 and 575 cm^{-1}, respectively, may belong to the bending vibration $\delta_{as}(SO_3)$ mixed with δ(C–C). Very weak bands of bending vibrations $\delta_s(SO_3)$ and $\rho(SO_3)$ are not found.

The stretching vibration (C)O–H of phenolic group cause the appearance of a mid broad band at 3151–3250 cm^{-1} (SC4, Fig. 3a), 3228–3251 cm^{-1} (SC6, Fig. 3b) and 3270–3340 cm^{-1} (SC8, Fig. 3c). In the IR spectrum of crystalline dihydrate of 2-hydroxy-4-methylbenzoic acid the contour of corresponding (C)O–H band is slightly narrower, and it has a maximum at 3189 cm^{-1} [21]. The

presence of the (C)O–H band in the IR spectrum interferes with the determination of stretching vibrations ν(OH) bands of proton hydrates. Its maximum is practically coincides with the maximum of ν(OH) of ions $H_5O_2^+$.

An evidence of neutral self-associates formation of H_2O molecules, like self-associates of liquid water, appear at a low humidity. Proton does not affect on their formation. A shoulder at 3393 cm^{-1} (SC4, RH = 20%, Fig. 3a), 3337 cm^{-1} (SC6, RH = 20%, Fig. 3b) and 3450 cm^{-1} (SC8, RH = 32%, Fig. 3c) , which appears on the ν(C–OH) contour, evidences about the presence of self-associated water molecules that are not influenced by proton. At the highest of RH intensive maximum of the broad absorption band of water at ~3400 cm^{-1} (Fig. 3a, c) is detected. The shoulder at 3360 cm^{-1} is observed instead of maximum in the case of SC6 (Fig. 3b). Humidification of samples leads to the appearance of neutral water molecules in a hydration shell, thereby forming the maximum δ(HOH) at 1651 cm^{-1} (SC4, RH ≥ 75%), 1638 cm^{-1} (SC6, RH ≥ 75%) and 1660 cm^{-1} (SC8, RH ≥ 54%) as well as the maximum at ~3400 cm^{-1} (SC4, RH ≥ 54%) or a remarkable shoulder at 3360 cm^{-1} (SC6 and SC8, RH ≥ 32%).

3.4 X-ray powder diffraction (XRD)

Figure 4a shows the diffraction patterns of the compound recorded at 54% RH. The peak intensities were low in all three samples, suggesting a low degree of crystallinity. All the samples have a heterogeneous structure, consist of two phases: crystalline and amorphous. More intensive peaks and a small halo are observed in the SC4 than in SC6 and SC8, so the former two last samples were less crystalline than the first one.

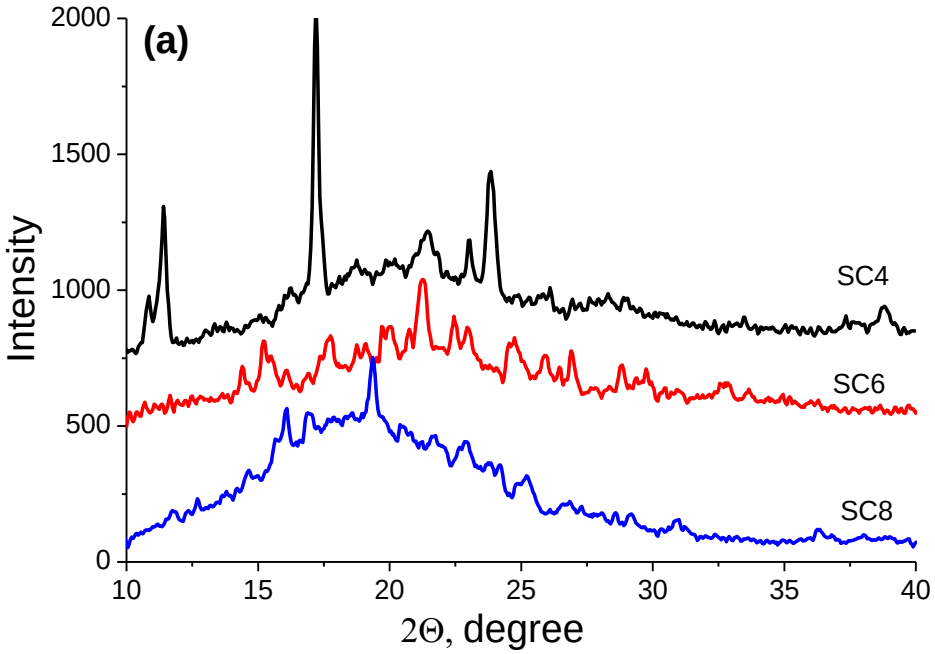

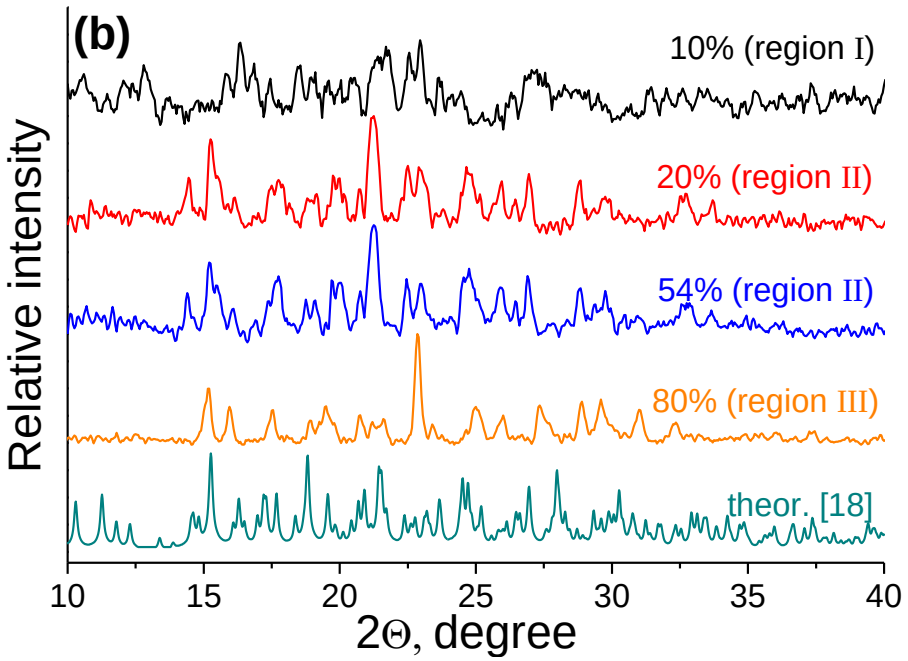

Figure 4. XRD spectra of SCn at 54% RH (a) and SC6 at different RH (b).

As was shown in our previous work [7] upon humidification we observed a shift of X-ray diffraction peaks toward small angles range that proves the existence of at least two crystalline hydrates of SC4.

Forms of crystalline part of the SC6 the spectra of SC6 upon dehydration (Fig. 4b) also prove the presence of several stages of hydration (see Fig. 1). The authors of work [19] showed that upon dehydration there was a decrease in the crystallinity of the SC6 suggesting the collapse of its crystal structure. This statement is consistent with our results.

3.4 Proton conductivity

Dependencies of the specific proton conductivities of SCn from their hydration degree have two types of characters (Fig. 5). The first type of conductivity has a very difficult dependence on water content in SC4, which correlates with the presence of two stable hydrates. The transition between hydrates does not entail a change in conductivity value, but within the hydrate a small water addition leads to a strong increase in the proton conductivity: from 2 to 26 and from 26 to 42 mS/cm. At a high water content the conductivity increases linearly with an increase in m (from 42 to 61 mS/cm).

The dependencies of proton conductivity for samples with n = 6 and 8 are significantly different from that for n = 4. They are well described by a power function with the critical index (the exponent) t = 6.0 and 6.8 for SC6 and SC8, respectively (Fig. 5):

$$\sigma = \sigma_0 \cdot m^t, \qquad (2)$$

where σ_0 is conductivity at m = 1. For both samples the values of σ_0 are close and equal to $3.7 \cdot 10^{-6}$ S/cm (SC6) and $1.2 \cdot 10^{-6}$ S/cm (SC8). In the terms of percolation theory it is better to use τ –

the dimensionless ratio that is characteristic of the closeness to the percolation threshold instead of *m* [26, 27]:

$$\tau = (m - m_c)/m_c, \quad (3)$$

where m_0 – percolation thresholds for the conductivity through crystallites. Extrapolation of the dependence in Fig. 5 was used to calculate m_0. For the structure of SC6 and SC8 estimated m_c is 3.6 water molecules per sulfonic group.

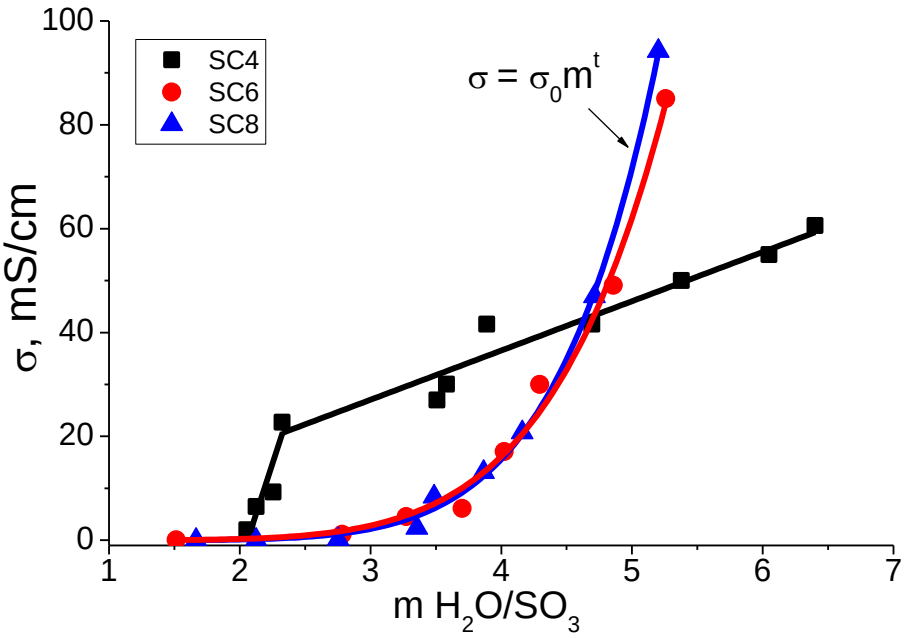

Figure 5. Proton conductivity dependencies of SCn on their hydration degree at 25 °C.

$$\sigma = \sigma_0 \cdot \tau^l. \quad (4)$$

It is evident that at low water content hydrogen bond network ceases to be continuous. Areas with different transport properties appear in the SCn structure. In the areas of high conductivity the proton transport occurs by the Grotthuss mechanism. Such areas have developed network of hydrogen bonds and, as a result, low energy barriers. The presence of water molecule bound with SO_3H-group leads to ionization of the latter and formation of H_3O^+, which becomes apparent in IR spectra (Fig. 3). So, between these areas proton transport takes place due to motion of oxonium ions by the vehicular mechanism and characterized by higher conductivity activation energy. To describe of such continuous conducting media consisting of areas with different transport characteristics the so-called hierarchical model of percolation structures is the most appropriate. So, in our work this model was used to theoretically estimate the critical index *l* in equation (4). For SC6 and SC8 *l* = 1.38 and 1.26, respectively, which corresponds to the hierarchical two-dimensional model (*l* = 1.3) [27, 28].

The proton conductivity dependence of SC4 on water content has linear character with an inflection at *m* = 2.3 and does not fit into the classical theory of percolation.

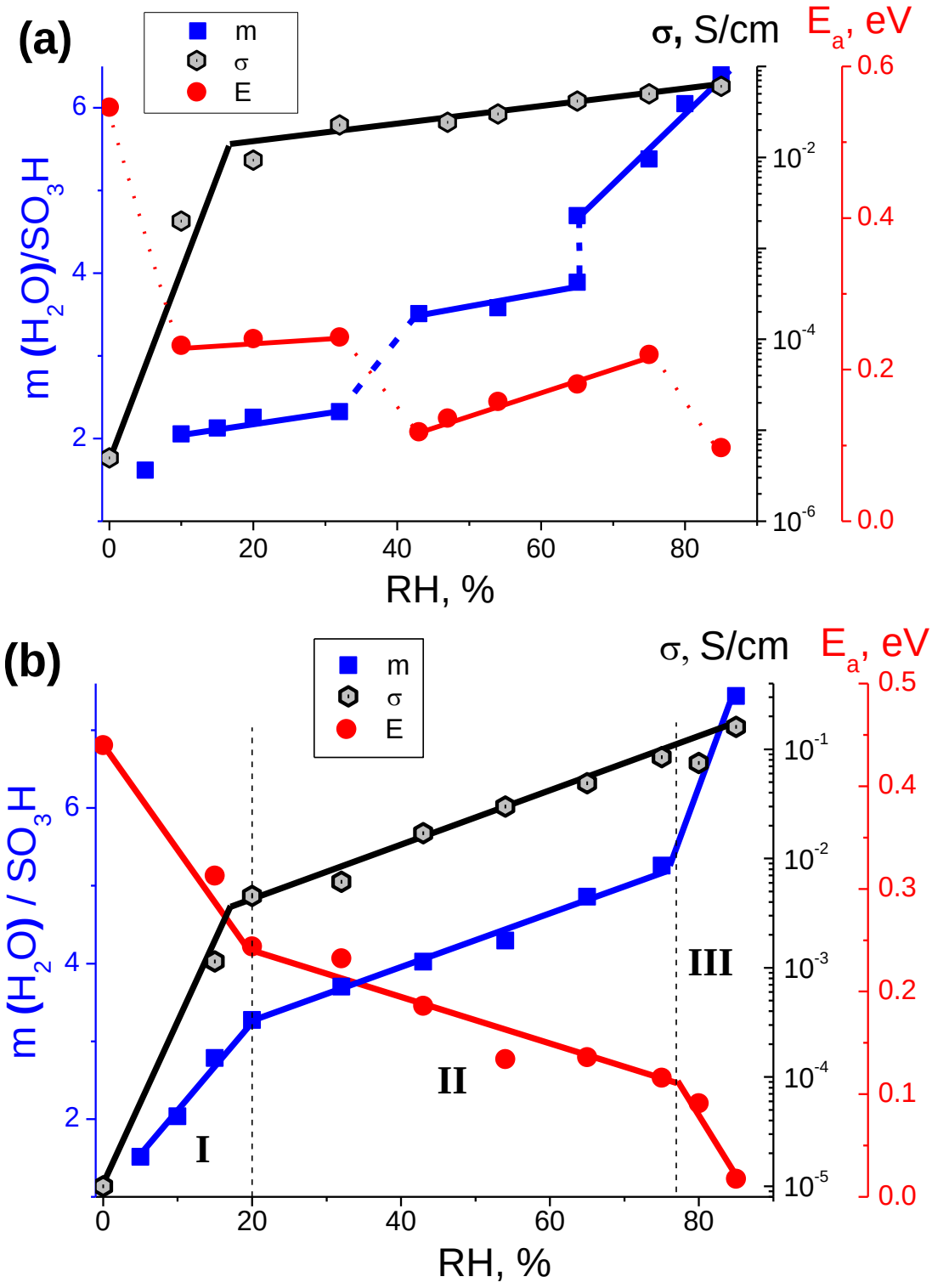
(a)
m
σ
E
σ, S/cm
E_a, eV
m (H2O)/SO3H
RH, %
(b)
m
σ
E
σ, S/cm
E_a, eV
m (H2O) / SO3H
I
II
III
RH, %

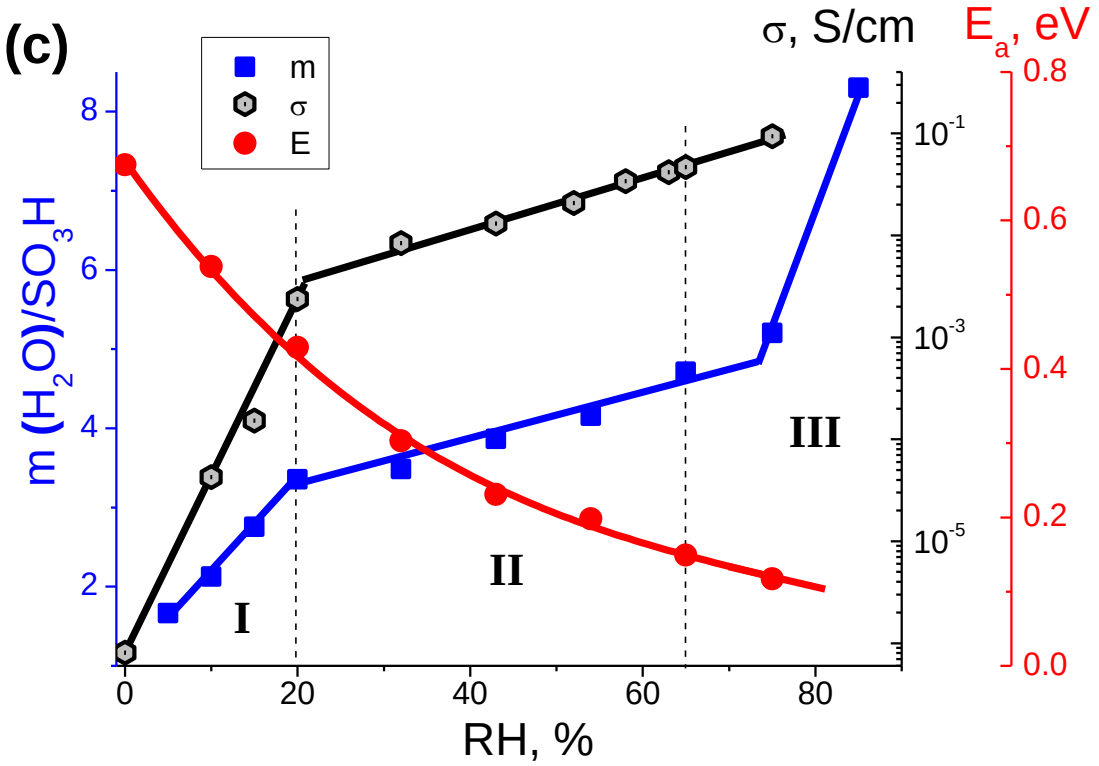

Figure 6. Water content (squares), proton conductivity (hexagons) and activation energy (circles) dependencies on RH for SCn at 25 °C: SC4 (a), SC6 (b), SC8 (c).

But the proton conductivity dependencies on RH are similar to each other (Fig. 6). Below 20% RH conductivity sharply increases by three to four orders of magnitude. Above 20% RH it hardly depends on the humidity.

The proton-conductivity activation energy also depends strongly on the amount of crystallization water and, consequently, from RH (Fig. 6). In general, the activation energy behavior during RH changing is different for all three samples.

In the case of SC4 (Fig. 6a), the activation energy of proton conductivity depends on humidity and varies from 0.23 to 0.10 eV in a complicated manner in accordance with the variation of the phase composition. In dry atmosphere, there was an anomalous growth of activation energy to 0.55 eV. In the range of existence of one crystalline hydrate phase, however, the activation energy of proton conductivity was not constant, in contrast to the value of conductivity, but increased with the water content. This unusual behavior is evidently explained by the fact that additional superstoichiometric water molecules within the existence of each crystalline hydrate greatly increase the barriers to the Grotthuss mechanism of proton transport in the hexagonal net of "stoichiometric" water molecules in the crystalline hydrate. The number of the additional molecules is rather small ($m \approx 0.3$). Proton transport occurs on the way both with increased and low energy barriers. The number of pathways with increased E_a and, therefore, experimentally measured effective value of activation energy increases during humidification [27].

Activation energy of SC6 and SC8 decreases monotonically with increasing of ambient humidity. At dry atmosphere the values of activation energy of SC6 decreases from 0.44 to 0.24 eV

(Fig. 6b, I region). The presence of inflection on the line at 20% RH apparently related to a reduction in the growth of water molecules in SC6 (II region), and, as a result, with change of the proton transport mechanism. The boundary of the transition to the III region is related to the formed an extensive network of hydrogen bonds with low energy barriers (0.11 eV at 75% RH), adding more of the molecules which does not lead to a change in the conduction mechanism. Thus, the antibate characters of water content and the conductivity activation energy show the effect of structural changes on the transport properties of SC6.

As for SC8, proton conductivity activation energy of the sample exponentially decreases upon wetting from 0.67 eV (0% RH) to 0.12 eV (75% RH) (Fig. 6c).

Thus, SCn for their proton transport properties are not inferior to the known low-temperature proton conductors. The values of proton conductivity and activation energy of some proton conductor containing sulfonic groups and heteropoly acids were shown in Table 2 and in reviews [29-31]. For example, proton conductivity of well known polymer membrane Nafion® in acid form [32-37] and sulfo phosphonates, which have a layered structure as SCn, [38-40] is 0.1 S/cm only at high humidity (90 – 100% RH). Proton conductivity of inorganic heteropoly acids with Keggin structure (without SO_3-group) reaches 0.2 S/cm also only at 95% RH [45-49]. In the case of SCn the same values are reached at lower humidity (75–85% RH).

Table 2. Proton conductivity and activation energy of some proton conductors.

Compound	**RH, %**	***T*, °C**	***σ*, mS/cm**	***E*$_a$, eV**	**Ref.**
SCn	20–85	25	4.6–160.5	0.24–0.12	This work
Nafion	20–100	33	1.2–95.0	0.10	[32-37]
Layered Zr and Ti sulfo phosphonates	85–90	20–22	13.0–100.0	0.20	[38-40]
SPEEK	 100	33 25	36.3 60.0	0.12	[32] [41]
Sulfonated fullerenols C_{60}	25–85	23	11.0	0.35–0.20	[42-44]
Heteropoly acids	32–75 95	25	2.0-20.0 200.0		[45-49]

3.6 NMR

3.6.1 Pulsed field gradient NMR

Self-diffusion coefficients (**SDC**) D_s of the test SCn (aged to constant weight at relative humidity of 32, 58, 65 and 75%) were measured by pulsed field gradient technique. In all cases the depending on the intensity of the signal "spin-echo" of the square of the amplitude of the magnetic field gradient (diffusion decay) [50-53] have a complicated configuration and can be well approximated by a sum of three exponential components by formula [50]:

$$A(g) = p_1 \cdot \exp(-\gamma^2 \cdot g^2 \cdot \delta^2 \cdot t_d \cdot D_{s1}) + p_2 \cdot \exp(-\gamma^2 \cdot g^2 \cdot \delta^2 \cdot t_d \cdot D_{s2}) + \\ + p_3 \cdot \exp(-\gamma^2 \cdot g^2 \cdot \delta^2 \cdot t_d \cdot D_{s3}), \quad (5)$$

where p_1, D_{s1}; p_2, D_{s2}; p_3, D_{s3} – relative fractions (phase population) and SDC of the first, second and third component, $A(g)$ – the intensity of the "spin-echo" signal, g – the amplitude of the magnetic field gradient, γ – gyromagnetic ratio of the investigated nuclei (^{1}H), δ – the duration pulse gradient, t_d – diffusion time.

Nonexponential character of the diffusion decay indicates the presence of heterogeneous regions (phases) in SCn, which translational mobility of $H^+(H_2O)_m$ complexes are different. Such heterogeneity may be caused by the presence of both amorphous and crystalline phases with different ionic mobility. Fig. 7 shows the diffusion decay of SCn, aged in an atmosphere of 58% RH. Analysis of the diffusion decays at different diffusion times (t_d was varied from 20 to 100 ms) showed the presence of the exchange between the phases. Thus, it has been shown (by the example of SCn at RH = 32%) that effective average SDC decreases from $4.3\cdot10^{-11}$ m^2/s (20 ms) to $2.8\cdot10^{-11}$ m^2/s (100 ms).

Average SDC was calculated by the formula:

$$D_s^{aver} = D_{s1}\cdot p_1 + D_{s2}\cdot p_2 + D_{s3}\cdot p_3 \qquad (6)$$

The averages SDC of SCn are presented in the Table 2. For all three samples there are observed a growth of SDC when the number of water molecules per sulfonic acid group increases. Studied calixarenes have similar values of SDC in all range of RH. For comparison of obtained data of diffusion with proton conductivity measured by the impedance spectroscopy σ_{theor} were calculated on the basis of the Stokes-Einstein relation:

$$\sigma = ze^2\frac{D}{kT}, \qquad (7)$$

where z – number of charge carriers per unit volume, e – electron charge ($1.9\cdot10^{-19}$ C), D – self-diffusion coefficient, m^2/s; k – Boltzmann's constant ($1.38\cdot10^{-23}$ J/K), T = 293 K – temperature. Values of the proton conductivity of calculated σ_{theor} and experimental σ_{exp} are presented in Table 3. Obtained data shows a good accordance for all SCn between the experimental and calculated values.

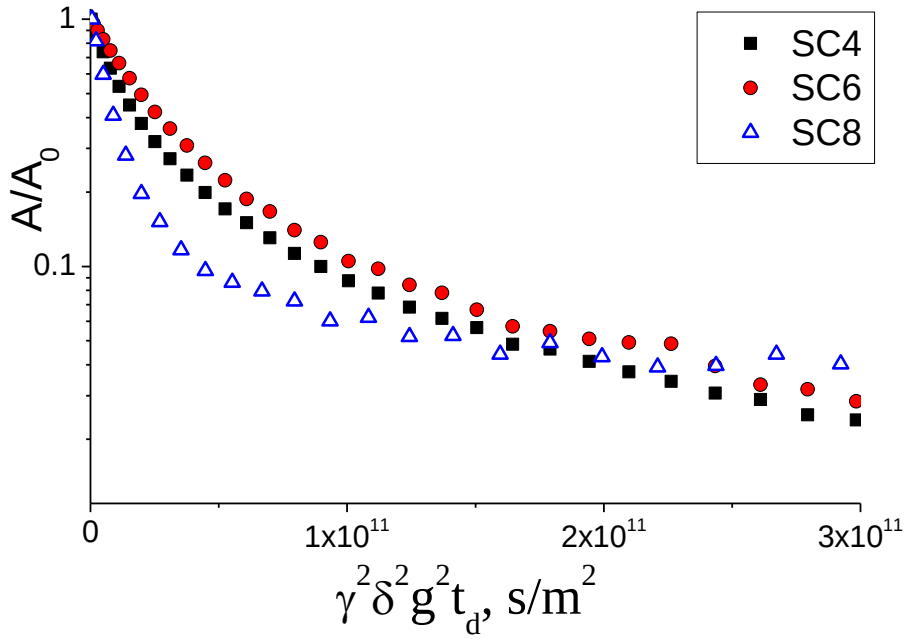

Figure 7. Diffusion decay of SCn (RH = 58%).

Table 3. Self-diffusion coefficients D_s^{aver}, values of the proton conductivity of SCn, experimentally measured σ_{exp} and theoretically-calculated from (7) σ_{theor}.

		32% RH	58% RH	65% RH	75% RH
D_s^{aver}, m^2/s	SC4	$3.7\cdot10^{-11}$	$7.0\cdot10^{-11}$	$1.2\cdot10^{-10}$	$1.3\cdot10^{-10}$
	SC6	$3.0\cdot10^{-11}$	$4.0\cdot10^{-11}$	$9.9\cdot10^{-11}$	$1.1\cdot10^{-10}$
	SC8	$1.7\cdot10^{-11}$	$7.2\cdot10^{-11}$	$1.3\cdot10^{-10}$	$1.5\cdot10^{-10}$
σ_{theor}, S/cm	SC4	$1.2\cdot10^{-2}$	$2.4\cdot10^{-2}$	$4.2\cdot10^{-2}$	$4.5\cdot10^{-2}$
	SC6	$1.0\cdot10^{-2}$	$1.4\cdot10^{-2}$	$3.4\cdot10^{-2}$	$3.8\cdot10^{-2}$
	SC8	$5.8\cdot10^{-3}$	$2.4\cdot10^{-2}$	$4.4\cdot10^{-2}$	$5.6\cdot10^{-2}$
σ_{exp}, S/cm	SC4	$2.0\cdot10^{-2}$	$3.0\cdot10^{-2}$	$4.2\cdot10^{-2}$	$5.0\cdot10^{-2}$
	SC6	$6.1\cdot10^{-3}$	$3.0\cdot10^{-2}$	$4.9\cdot10^{-2}$	$8.5\cdot10^{-2}$
	SC8	$8.4\cdot10^{-3}$	$1.8\cdot10^{-2}$	$4.7\cdot10^{-2}$	$9.4\cdot10^{-2}$

3.6.2 Solid state high resolution magic angle spinning NMR (MAS NMR)

To monitor the structural changes with increasing water molecules per sulfonic acid group in SCn the solid state NMR studies were carried out using the technique of magic angle spinning. Spectra of ^{13}C-CP/MAS (1H) (aged at RH = 10%) are presented in Fig. 8. At 31–32 ppm a broadened ^{13}C signal of bridge –CH_2– group is observed. In the range of 120–160 ppm - the carbon atoms of the aromatic ring signal. In the most downfield (> 150 ppm) the signal of carbon atoms from –C–OH group is observed, more to the right at 132–140 ppm – C-SO_3H, and signals in the range of 120–130 ppm correspond to the chemical shifts of the ^{13}C of –CH and –C–CH_2 groups.

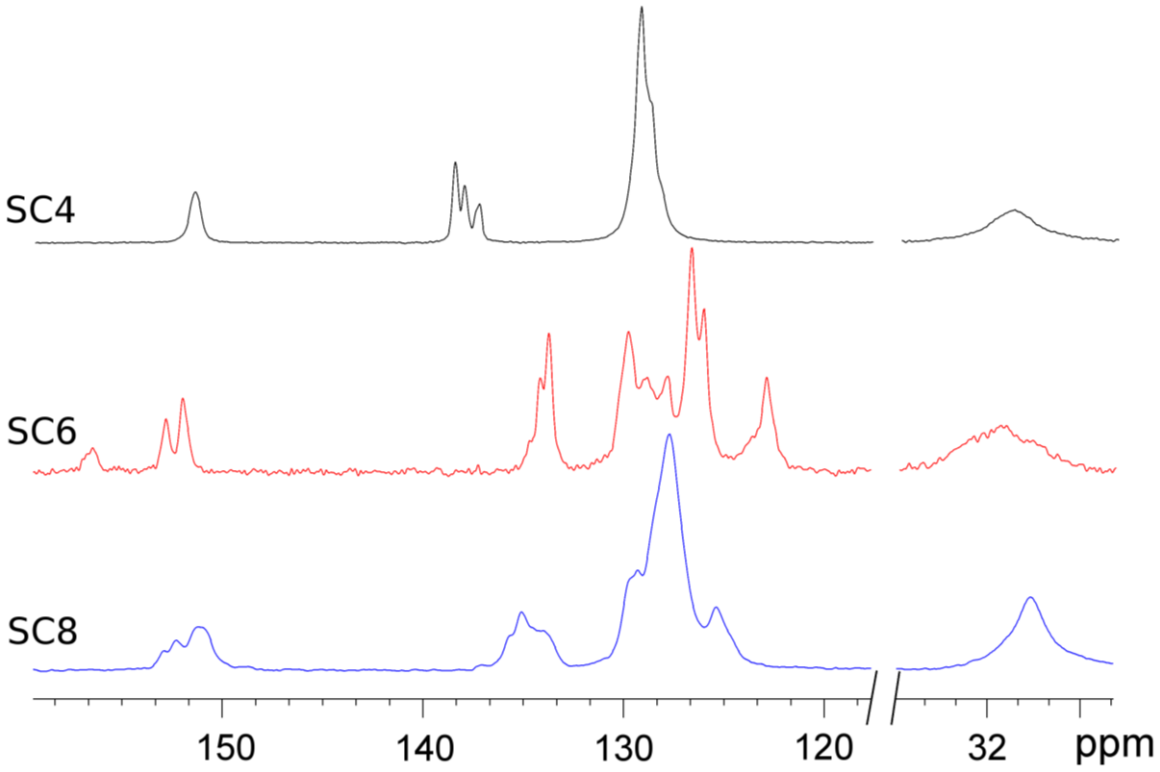

Figure 8. ^{13}C-CP(^{1}H) MAS NMR spectra of SCn (10% RH, spinning rate 13 kHz).

As is seen from spectra there are several signals for each signal group of carbon atoms of aromatic ring in case of SC6 and SC8. The presence of a large number of signals is due to the existence of calixarene rings with various conformations in the structure. For calixarene with the smallest size of the cycle - SC4 there is no appreciable complexity of the spectrum due to the conformational variety. Presumably, the cycles in the structure are particular in the "cone" conformation. This is confirmed by the signal position of $–CH_2–$ group in ^{13}C NMR spectrum. Thus, it is known from literature [54, 55] that in the different solutions of SC4, forming a cone conformation, a signal of $–CH_2–$ group in ^{13}C NMR spectrum is observed in the range of 31–33 ppm, rather than 36–39 ppm, which is specific for other conformational types. For calixarenes with large size of cycle a signal position of $–CH_2–$ group in ^{13}C NMR spectrum does not allow to determine conformation [56].

Fig. 8a displays that the ^{13}C NMR signal of $–\underline{C}–SO_3H{\cdot}mH_2O$ group in SC4 consists of several lines, which is caused by non-uniform distribution of water molecules in the sulfonic acid groups. At moistening of SC4 a distribution of water molecules in the sulfonic acid groups becomes uniform. ^{13}C NMR signal of $–\underline{C}–SO_3H{\cdot}mH_2O$ group in SC4 (aged at RH = 32%, Fig. 9a) is one narrow signal. Also it has been shown that as number of the water molecules in SC6 and SC8 increases (Fig. 8 and 9), respectively) the ^{13}C NMR spectra are almost not changed.

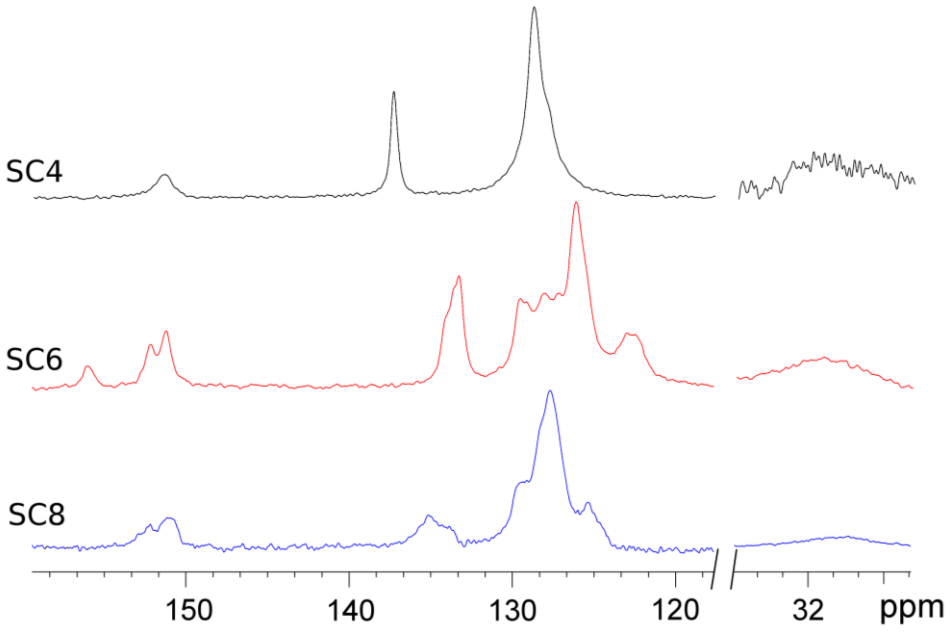

Figure 9. ^{13}C-CP(^1H) MAS NMR spectra of SCn (32% RH, spinning rate 13 kHz).

Fig. 10a shows the spectrum of SC4, which was dried at 120 °C for 2 days. As seen from the spectrum, a removal of most of the water from the structure causes a change in signals of all types of carbon atoms. At the transition from RH = 32% to 10% we observed a change in only carbon atoms of "upper rim" calixarenes cup in the spectrum, now removal of water caused a change in the "lower rim» of SC4. This change may be caused by the removal of water from layer formed hydroxyl groups or appearance of conformational flexibility, which caused by destruction of the intermolecular hydrogen bonds.

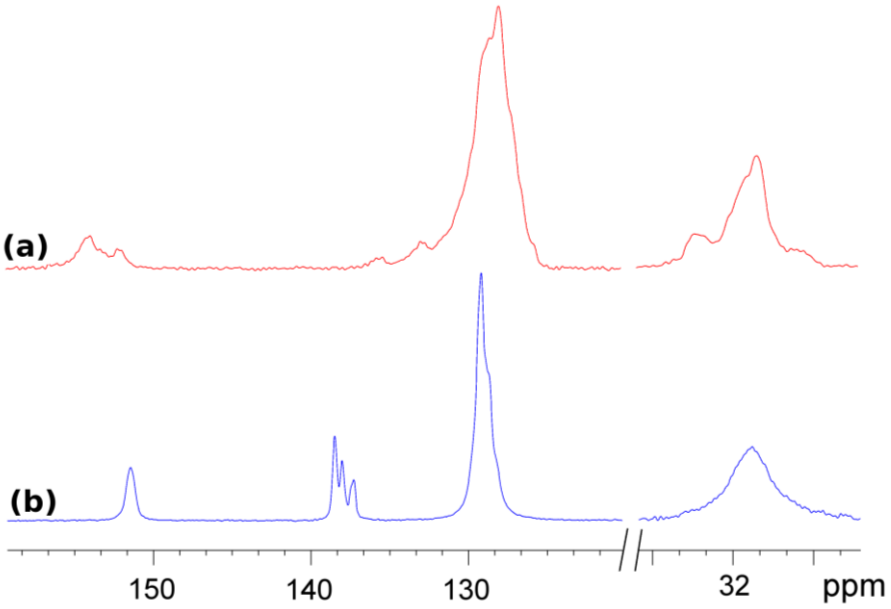

Figure 10. ^{13}C-CP(^{1}H) MAS NMR spectra of SC4, dried at 120 °C for 2 days (a) and at relative humidity (b) RH = 10% (spinning rate 13 kHz).

4. CONCLUSIONS

In summary, the influence of the morphology of calix(n)arene sulfonic acid hydrates with different number of aromatic rings (*n* = 4, 6, 8) on their proton transport properties was studied. In all the samples the hydrate water content increases during ambient humidity increasing. Dehydration process occurs in several stages up to 150 °C. IR spectroscopy data shows that under low RH conditions calix(n)arene sulfonic acids are not absolutely dehydrated. Moreover, sulfonatocalix(4)arene has one H_2O molecule per SO_3–group even under vacuum.

XRD and NMR analyses show that all the samples have a heterogeneous structure, consist of crystalline and amorphous phases. Calixarene with the smallest size of the cycle (*n* = 4) is not only more crystalline, but has only one “cone” conformation. In the range of 32–75% RH the average SDC of all the samples increase from 10^{-11} to 10^{-10} m^2/s.

Proton conductivities and activation energies of calix(n)arene sulfonic acids were studied. The proton conductivity dependence of sulfonatocalix(4)arene on its hydrate water content has a difficult character. The dependence of proton conductivity of the samples on water content has a power character with the critical index *t* = 6.0 and 6.8 for n = 6 and 8, respectively. It was shown that the values of conductivity reach 10^{-1} S/cm (75% RH) for all the compounds and activation energy decreases up to 0.1 eV.

So, such compounds are very perspective material for various electrochemical devices, such as fuel cells and gas sensors.

ACKNOWLEDGEMENTS
This work was supported by Russian Scientific Foundation (Contract No. 14-23-00218).

References

1. Yu. A. Dobrovolsky, E. V. Volkov, A. V. Pisareva, Yu. A. Fedotov, D. Yu. Likhachev and A. L. Rusanov, *Russ. J. General Chem*., 77 (2007) 766.
2. A. V. Yaroslavtsev, Yu. A. Dobrovolsky, N. S. Shaglaeva, L. A. Frolova, E. V. Gerasimova and E. A. Sanginov, *Russ. Chem. Rev*., 81 (2012) 191.
3. A. D. Martin and C. L. Raston, *Chem. Commun*., 47 (2011) 9764.
4. L. V. Shmygleva, A. V. Pisareva, R. V. Pisarev, A. E. Ukshe and Yu. A. Dobrovol'skii, *Russ. J. Electrochem.*, 49 (2013) 801.
5. A. E. Ukshe, L. V. Shmygleva, N. G. Bukun and Yu. A. Dobrovolsky, *Russ. J. Electrochem*., 49 (2013) 807.
6. A. V. Pisareva, R. V. Pisarev, A. I. Karelin, L. V. Shmygleva, I. S. Antipin, A. I. Konovalov, S. E. Solovieva, Yu. A. Dobrovolsky and S. M. Aldoshin, *Russ. Chem. Bull*., 61 (2012) 1892.
7. L. V. Shmygleva, E. A. Sanginov, R. R. Kayumov, A. E. Ukshe and Yu. A. Dobrovol'skii, *Rus. J. Electrochem*., 51 (2015) 468.
8. J. L. Atwood, A. W. Coleman, H. Zhang, and S. G. Bott, *J. Inclusion Phenom. Molec. Recogn. in Chem.*, 7 (1989) P. 203.
9. R.-G. Lin, L.-S. Long, R.-B. Huang, and L.-S. Zheng, *Inorg. Chem. Commun*., 10 (2007) 1257.
10. S. J. Dalgarno, and C. L. Raston, *Dalton Trans*., 3 (2003) 287.
11. Y.-M. Legrand, A. Van der Lee and M. Barboiu, *Science*., 329 (2010) 299.
12. Z. Asfari, J. Harrowfield, P. Thuery and J. Vicens, *Supramol. Chem*., 15 (2003) 69.
13. Y. Israeli, G. P. Yap and A. C. Detellier, *Supramol. Chem*., 12 (2001) 457.
14. S. J. Dalgarno, J. L. Atwood and C. L. Raston, *Cryst. Growth Des*., 7 (2007) 1762.
15. J. L. Atwood, L. J. Barbour, S. Dalgarno, C. L. Raston and H.R. Webb, *J. Chem. Soc., Dalton Trans.*, 2002. V. 23. P. 4351.
16. J. L. Atwood, D. L. Clark, R. K. Juneija, G. W. Orr, K. D. Robinson and R. L. Vincent, *J. Am. Chem. Soc*., 114 (1992) 7558.
17. J.-P. Scharff, M. Mahjoubi and R. Perrin, *New. J. Chem*., 15 (1991) 883.
18. V. I. Volkov, S. A. Korotchkova, H. Ohya and Q. Guo, *J. Membr. Sci.*, 100 (1995) 273.
19. W. Yang, R. Manek, W.M. Kolling, M.B., W. Liebenberg and M.M. De Villiers, *Supramol. Chem*., 17 (2005) 485.
20. A. V. Pisareva, G. V. Shilov, A. I. Karelin and Yu. A. Dobrovolsky, *Russ. J. Phys. Chem*., 82 (2008) 355.
21. A. V. Pisareva, G. V. Shilov, A. I. Karelin, Yu. A. Dobrovolsky and R. V. Pisarev, *Russ. J. Phys., Chem.* A., 84 (2010) 444.
22. V. Pisareva, G. V. Shilov, A. I. Karelin, R. V. Pisarev and Yu. A. Dobrovolsky, *Russ. Chem. Bull.*, 57 (2008) 364.
23. E. Zundel. Hydration and intermolecular interaction. New York: Academic Press, 1969.
24. H. T. Varghese, C. Y. Panicker and D. Philip, *J. Raman Spectrosc*., 38 (2007) 309.
25. V. L. Furer, E.I. Borisoglebskaya and V. I. Kovalenko, *Spectrochimica Acta: Part* A, 61 (2005) 355.
26. V. L. Furer, L. I. Potapova and V. I. Kovalenko, *J. Molec. Structure*, 112 (2017) 439.
27. A. A. Snarskii, I. V. Bezsudnov and V. A. Sevryukov. Protsessy perenosa v makroskopicheski neuporyadochen nykh sredakh: Ot teorii srednego polya do perkolyatsii (Transport Processes in Macroscopic Disordered Media: From the Mean_field Theory to percolation), Moscow: LKI, 2007.
28. B. I. Shklovskii and A. L. Efros. Elektronnye svoistva sil'no legirovannykh poluprovodnikov (Electronic Properties of Heavily Doped Semiconductors), Moscow: Nauka, 1979.
29. P. Ramaswamy, N. E. Wong and G. K. H. Shimizu, *Chem. Soc. Rev*., 43 (2014) 5913.
30. J. W. Phair andS. P. S. Badwal, *Ionics*12 (2006) 103.
31. A. V. Pisareva and R. V. Pisarev, *Int. Sci. J. .Altern. Energy and Ecology*, 12 (2007) 105.

32. A. Shukla, S. D. Bhata and V. K. Pillai, *J. Membr. Sci*., 520 (2016) 657.
33. L. Maldonado, J.-C. Perrin, J. Dillet and O. Lottin, *J. Membr. Sci*., 389 (2012) 43.
34. H. Wang , B. A. Holmberg, L. Huang, Z. Wang, A. Mitra, J. M. Norbeck and Y. Yan, *J. Mater. Chem.*, 12 (2002) 834.
35. E. L. Thompson, T. W. Capehart, T. J. Fuller and J. Jorne, *J. Electrochem. Soc*., 153 (2006) A2351.
36. V. Ch. Bokun , D. A. Kritskaya, E. F. Abdrashitov, A. N. Ponomarev, E. A. Sanginov, A. B. Yaroslavtsev and Yu. A. Dobrovol'skii, *Russ. J. Electrochem*., 51 (2015) 435.
37. R. R. Kayumov, L. V. Shmygleva and Yu. A. Dobrovolsky, *Russ. J. Electrochem*., 51 (2015) 556.
38. G. Alberti, M. Casciola, U. Costantino, A. Peraio and E. Montoneri, *Solid State Ionics*, 50 (1992) 315.
39. E. W. Stein Sr., A. Clearfield and M. A. Subramanian, *Solid State Ionics*, 83 (1996) 113.
40. G. Alberti, U. Costantino, M. Casciola, S. Ferroni, L. Massinelli and P. Staiti, *Solid State Ionics*, 145 (2001) 249.
41. Z. Wang, H. Ni, C. Zhao, X. Li, T. Fu and H. Na, *J. Polym. Sci., Part B: Polym. Phys*. 44 (2006) 1967.
42. J. Gasa, H. Wang, R. DeSousa and K. Tasaki, *ECS Transactions*, 11 (2007) 131.
43. K. Tasaki, A. Venkatesan, H. Wang, B. Jousselme, G. Stucky and F. Wudl, *J. Electrochem. Soc*., 155 (2008) B1077.
44. L. V. Shmygleva, A. V. Pisareva, E. A. Ukshe, R. V. Pisarev, A. B. Kornev, P. A. Troshin and Yu. A. Dobrovolsky, Organic proton conductorsbased on fullerene C60 derivatives,13th International Meeting "Fundamental problems of solid state ionics", Chernogolovka, Russia, 2016, 336.
45. A. Chikin, A. Chernyak, Zh. Jin, Yu. Naumova, A. Ukshe, N. Smirnova, V. Volkov and Yu. Dobrovolsky, *J. Solid State Electrochem*., 16 (2012) 2767.
46. L. A. Fisun and V. N. Pak, *J. Appl. Chem. USSR*, 65 (1992) 213.
47. A. Hardwick, P. G. Dickens and R. C. T. Slade, *Solid State Ionics*, 13 (1984) 345.
48. K. D. Kreuer, M. Hampele, K. Dolde and A. Rabenau, *Solid State Ionics*, 28 (1988) 589.
49. O. Nakamura, I. Ogino and T. Kodama, *Solid State Ionics*, 3-4 (1981) 347.
50. A. I. Maklakov, V. D. Skirda and N. F. Fatkullin. Self-Diffusion in Polymer Solutions and Melts. Kazan: Kazan State University Press, 1987
51. P. T. Callaghan. Principle of NMR Microscopy. Oxford: Clarenden Press, 1991.
52. C.-H. Cho, Y.-S. Hong, K. Kang, V.I. Volkov, V. Skirda, C.-Y.J. Lee and C.-Ho Lee, Magnetic Resonance Imaging, 21 (2003) 1009.
53. K.-J. Suh, Y.-S. Hong, V. D. Skirda, V. I. Volkov, C.-Y. J. Lee and C.-H. Lee, *Biophys. Chem*., 104 (2003) 121.
54. C. Jaime, J. de Mendoza, P. Prados, P. M. Nieto and C. Sanchez, *J. Org. Chem*., 56 (1991) 3372.
55. C. David Gutsche, Calixarenes An Introduction. 2nd Edition. Tucson: University of Arizona, RSC, 2008.
56. T.-M. Liang and K. K. Laali, *Chem. Ber*., 124 (1991) 2637.